IEEE Access
Multidisciplinary | Rapid Review | Open Access Journal

Received July 28, 2020, accepted August 5, 2020, date of publication August 10, 2020, date of current version August 20, 2020.

Digital Object Identifier 10.1109/ACCESS.2020.3015195

Underwater Pressure and Temperature Sensor Based on a Special Dual-Mode Optical Fiber

XUEQIN LEI[1], XIAOPENG DONG[1], CHENXU LU[1], TONG SUN[2], AND KENNETH T. V. GRATTAN[2]

[1]School of Electronic Science and Engineering, Institute of Lightwave Technology, Xiamen University, Xiamen 361005, China
[2]School of Mathematics, Computer Science and Engineering, City, University of London, London EC1V 0HB, U.K.

Corresponding author: Xiaopeng Dong (xpd@xmu.edu.cn)

This work was supported in part by the National Natural Science Foundation of China under Grant 61775186, in part by the Fujian Provincial Department of Science and Technology under Grant 2014H6027, and in part by the Marine and Fisheries Bureau of Xiamen under Grant 16CZB025SF03. The work of Tong Sun and Kenneth T. V. Grattan was supported by the Royal Academy of Engineering.

ABSTRACT In this paper, an all fiber optic sensor based on a Mach-Zehnder interferometer (MZI) has been proposed for the simultaneous measurement of underwater pressure and temperature, utilizing a dual-mode fiber (DMF) which has been specially designed, and supporting only the LP_{01} and LP_{02} modes propagating in the fiber. In this design, an in-line MZI sensor that was constructed by splicing a DMF between two pieces of single mode fibers, shows a critical wavelength (CWL) which exists in the transmission spectrum of the LP_{01}-LP_{02} mode interference. Since the two peaks, located closest to the CWL (and from both lower and higher wavelengths), shift in opposite directions and show different sensitivities under temperature and water pressure variations, the DMF-MZI sensor is capable of measuring both the water pressure and the temperature simultaneously. The CWL-based interference spectrum is stable with the variation of underwater salinity or impurities seen around the fiber surface and independent of the polarization states of the transmission light. As a result, in the operation of the DMF-MZI sensor, underwater pressure and temperature sensitivities increase significantly, when the peak wavelengths are close to that of the CWL. A theoretical analysis has been developed and used to predict that the sensitivities of this specific DMF-MZI structure which can be further improved by increasing the physical length of the DMF and by adjusting the position of the first left/right peak to be closer to the critical wavelength. This co-located, multi-parameter all-fiber sensor developed in this way and showing relatively high sensitivity is easy to implement in the underwater environment. It does not require a complex shell design and the peaks nearest to a CWL are convenient, allowing easy identification and detection, thereby providing a large measurement range to satisfy the requirements of practical marine and fresh water measurements.

INDEX TERMS Fiber sensor, temperature, pressure, dual mode fiber, Mach-Zehnder interferometer.

I. INTRODUCTION

An accurate knowledge of temperature of seawater is one of the most important parameters in oceanology and a critical driving factor in ocean dynamics today [1]. Further, fast and accurate measurements of underwater depth are particularly important for building a precise profile of the seawater temperature. However, the conventional, expendable temperature/depth profiler (XBT) probe available and which is based on the use of a thermistor, can allow the depth data to be obtained only by calculating this from the speed and time information and using an algorithm, rather than allowing a direct, more accurate measurement. Conductivity, temperature, and depth sensor systems (CTDs), which include a piezoelectric sensor, can be used to detect the temperature data which can be related to the depth of seawater: however, these devices are costly, complex and in general bulky. In contrast to their electronic counterparts, fiber-optic temperature/depth sensors exhibit the outstanding advantages of compactness, fast response, low cost and immunity to electromagnetic interference. Such an innovative sensor scheme is the subject of this work.

Currently, various all-fiber detection schemes have been proposed for measuring water pressure (depth) and temperature, simultaneously. Traditional barometric pressure fiber optic sensors [2]–[5], which commonly are constructed with

The associate editor coordinating the review of this manuscript and approving it for publication was Kin Kee Chow.

open cavities, trenches or holes fabricated by chemical etching or laser micro-machining techniques (to allow the media on which the measurements are made easy to be placed within (and removed from) the FPI cavity used), may not be well suited to marine applications, because these etched structures are thus physically weakened and may be fragile: so they may be sensitive to ambient environmental vibrations, and errors also can occur in their use due to the variation of the salinity of the seawater or the presence of contaminants from the water samples in the open FPI cavities thus created. Measuring errors also exist in fiber in-line Mach-Zehnder Interferometer (MZI) designs, which have a common characteristic of RI sensitivity to the liquid analyte: thus the following features 1) the sensor is used with a bare fiber core [6]; and 2) a thin clad fiber structure, which has a large evanescent field exposed to the surrounding [7]; 3) the sensor is based on cladding mode and core mode interference, which usually is formed by employing two heterogenic fibers (e.g., multimode fiber [8] or PCF [9]) or abnormal fiber fusion splicing (e.g., core offset [10], S-shaped [11] or peanut-like [12] arrangements), used to excite the high order/cladding modes propagating in the sensing fiber, which lead to a relatively large energy spread out of the doped core – as a result, the silica cladding acts as the ''core'' of the sensing structure. In light of this, noting previous work where similar cases were seen and where extrinsic FP cavity structures were proposed [13]–[17], particular attention needs to be paid to the use of specialized materials and the process of packaging shell design, essential for marine applications. All of this significantly increases the cost and difficulty of fabrication.

Moreover, the multimode interference created may decrease the uniformity and clarity of the interference spectrum created, and several interferometers in a cascaded configuration (as proposed in the literature [2]–[5], [18], [19]) often then form a complicated structure. Both the multimode interference and interferometers-cascaded schemes create multiple interference signals and thus require a high degree of complexity in the signal analysis and interrogation processes needed, due to the interference fringes with similar periods which are seen to overlap in the spectrum obtained. In addition, the Fiber Bragg Grating-based schemes proposed in the literature [20]–[22] still show problems due to the system complexity, instability and relatively short lifetime when used in practical applications, because of the combination of pressure sensitive materials or the different geometric structures used (e.g., the thin walled cylinders, the polymer diaphragm or the diaphragm-cantilever structures). Therefore, alternative approaches to create a more appropriate sensor design are needed, tailored better to the applications in this work in the underwater environment.

In this article, a compact fiber in-line dual-mode fiber (DMF) Mach-Zehnder interferometer (MZI) designed for the simultaneous water pressure and temperature measurement is presented. The DMF employed in this approach has been specially designed to support only the fundamental mode, LP_{01}, and the higher order core mode, LP_{02}, propagating in the fiber [23]. This is different from the conventional few mode fiber approach, in which several higher order core modes (e.g., LP_{11}) are supported. Here the DMF used in this sensor structure is superior in its polarization behavior [24] and it is stable, even with the variation of the contaminants experienced in the underwater environment. As reported in our previous work [25], the propagation constant difference between the LP_{01} and the LP_{02} modes, $\Delta\beta$, has a maximum corresponding to the critical wavelength (CWL) in the transmission spectrum. The peaks that lie closest to the CWL on each side have their maximum spacing from the adjacent peaks, which can readily be identified in the interference spectrum. Moreover, due to fact that the peaks which are closest to the CWL on each side shift in opposite directions, (having different strain and temperature sensitivities [26]), a high resolution in the measurement of co-located dual-parameters was made possible by monitoring the shifts of the observed 'Right Peak1' and 'Left Peak1' seen respectively in the spectrum obtained. This approach has been extended to form the basis of the sensor design discussed in this current work.

In our previous research, the interferometers used and based on the DMF approach have functioned to monitor various measurands: as a displacement sensor [27], a refractive index sensor [28], and a humidity sensor [29], for example. In this paper, the unique characteristics of this approach are presented as the basis of a simultaneous water pressure/depth and temperature measurement system for application in the marine or fresh water environments. The DMF-MZI structure proposed, based on two core-mode interference, can readily be fabricated by splicing a piece of DMF between two segments of single mode fibers (SMFs). This simple DMF-MZI configuration for dual-parameter measurement also allows several advantages over these alternative approaches to be shown, which include: 1) it is simple, robust and low cost, when compared to the fiber grating-inscribed schemes for temperature compensation, which may require an additional processing stage, such as high-pressure hydrogen-loading or a laser machining approach; 2) it uses relatively low optical loss compared to other non-standard spliced fiber in-line arrangements, such as suspended core fiber [30], thin core fiber [31], dual-core photonic crystal fiber [32], [33] or other lateral shifted splicing structures – it is essential for long distance operation to have low optical loss; 3) it is easy to implement and the peaks nearest to a CWL are conveniently used for identification and detection, when compared to the cladding-mode-excited all fiber in-line sensor structures – generally showing a similar uniform interference spectrum, easily disturbed by the variation of the refractive index of seawater and then requiring a special design of the 'packaging' of the sensor for the applications in the marine environment; 4) a wide measurement range and good linearity for deep water measurement is seen, compared to the traditional FP pressure sensor structures, whose measurement range and sensitivity are limited in a variable length of resonance cavity, as well as the deformation of the diaphragm materials or other geometric constructions

used [13], [14], [18]–[22]: these may exhibit a nonlinear relationship between the depth or pressure and the sensitivity; 5) a relatively high sensitivity is characteristic of these sensors, where the maximum pressure sensitivity obtained in experiments carried out is 1-3 orders of magnitude larger than is seen in dual-core fiber, PCF or FBG-based pressure sensors reported in the literature [32], [33], [20]. This design could be further improved by increasing the physical length of the DMF, using this characteristic in the prediction of the experimental measurements or the results of simulation. As a result, the all fiber sensor device discussed shows promising and significant prospects for use in making simultaneous underwater pressure and temperature measurements, implemented in different practical applications.

II. OPERATIONAL PRINCIPLE OF THE SENSOR

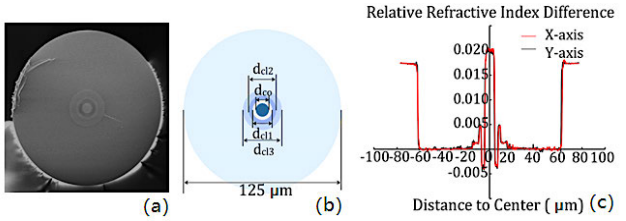

FIGURE 1. Configuration and index profile of the DMF. (a) SEM micrograph of the DMF; (b) Geometrical structure of the DMF; (c) Relative refractive index difference profile of the DMF, measured at a wavelength of 670nm.

The DMFs used in the experimental verification were provided by the Yangtze Optical Fiber and Cable Limited Company Ltd, and a scanning electron microscope (SEM) micrograph of the fiber itself is shown in Fig. 1(a). The DMFs employed here were specially designed using a highly GeO_2-doped inner core, three inner claddings, and a pure silica outer cladding to ensure that only the fundamental mode, LP_{01}, and the higher order core mode, LP_{02}, were allowed to propagate along the fiber. The multi-layer geometrical structure and the W-shaped refractive index difference profile of the DMF used is shown in Fig.1 (b) and (c). In the experiment carried out, the Mach-Zehnder interferometer (MZI) was formed by splicing a section of the DMF between two pieces of SMFs. The LP_{01} and LP_{02} modes that propagate in the DMF were excited by the fundamental core mode, LP_{01}, in the input SMF. The interference between the LP_{01} and LP_{02} modes was selected by using the output SMF. If the optical power ratios transferred from the input SMF to the LP_{01} and LP_{02} modes are t_{01} =P_{01}/Pin and t_{02} =P_{02}/Pin, respectively, then the transmission through the DMF is given simply as follows [34]:

$$T = P_{out}/P_{in} = t_{01}^2 + t_{02}^2 + 2t_{01}t_{02}\cos(\varphi(\lambda)) \tag{1}$$

where $\varphi(\lambda)$ is the phase difference developed between the LP_{01} and LP_{02} modes in the DMF with a physical length, L, which is represented as follows:

$$\varphi(\lambda) = \Delta\beta(\lambda)L \tag{2}$$

where $\Delta\beta = \beta_{01} - \beta_{02}$ is the propagation constant difference between the LP_{01} and LP_{02} modes. β_{01} and β_{02} are the propagation constants of the LP_{01} and LP_{02} modes in the DMF, respectively. The phase difference between the LP_{01} and LP_{02} modes is a function of both the operating wavelength, λ, and the perturbation parameter, χ (temperature or pressure), as shown in Equation (2). Therefore, the change in the phase difference can be expressed as [35]:

$$\Delta\varphi = \frac{\partial\varphi}{\partial\lambda}\Delta\lambda + \frac{\partial\varphi}{\partial\chi}\Delta\chi \tag{3}$$

For a constant phase point, we have:

$$\frac{\Delta\lambda}{\Delta\chi} = -\frac{1}{L}\left(\frac{\partial\varphi}{\partial\chi}\right)\left(\frac{\partial(\Delta\beta)}{\partial\lambda}\right)^{-1} \tag{4}$$

where $\partial\varphi/\partial\chi$ is the phase difference induced by the pressure or temperature that was applied. L is a positive quantity at the operational wavelength, λ. With the fiber parameters given in Fig.1 and a core refractive index of 1.473, using the finite element analysis method, the calculated transmission spectrum of the DMF-MZI structure, of 0.34m length DMF, combining (1) and $\Delta\beta$, is shown as the solid line in Fig. 2(a). The corresponding experimental transmission spectrum is depicted in Fig. 2(b), which is consistent with the simulated results obtained. As shown in Fig. 2, numbering from the peaks that lie closest to the CWL from both sides, the peaks on the right-hand side of CWL are denoted by P_{R1}, P_{R2}, ..., respectively. The peaks that are located on the left-hand side of CWL are denoted as P_{L1}, P_{L2}, ..., respectively. $\partial(\Delta\beta)/\partial\lambda$ is positive on the lower wavelength side of the CWL, while negative on the longer wavelength side of the CWL [26], which leads to an opposite shift of the peaks located on the both sides of the CWL, with a change in the temperature/water pressure. The spacing between the peaks/dips that lay closest to the CWL on each side and the adjacent peaks/dips is the maximum compared to rest, so they can be easily identified from the observed interference fringes. As a consequence, the change of the ambient temperature or the pressure (due to the water depth) can be monitored by tracing the wavelength shift of the peaks in the interference spectrum.

Both the pressure-induced refractive index change and the pressure-induced structural deformation will be affected by the hydrostatic pressure applied to the optical fiber, thus affecting the light guidance in the optical fiber. Based on the well-known photo-elastic effect, the refractive index of the silica under the hydrostatic pressure can be expressed as follows [36]:

$$\begin{aligned}\Delta n_x &= -C_1\sigma_x - C_2(\sigma_y + \sigma_z)\\ \Delta n_y &= -C_1\sigma_y - C_2(\sigma_x + \sigma_z)\\ \Delta n_z &= -C_1\sigma_z - C_2(\sigma_x + \sigma_y)\end{aligned} \tag{5}$$

where σ_x, σ_y and σ_z are the stress components in the X, Y and Z axes, $C_1 = 6.5 \times 10^{-13} m^2/N$ and $C_1 = 4.2 \times 10^{-12} m^2/N$ are the stress-optic coefficients of pure silica. The stress components of the silica can be determined, based on the results

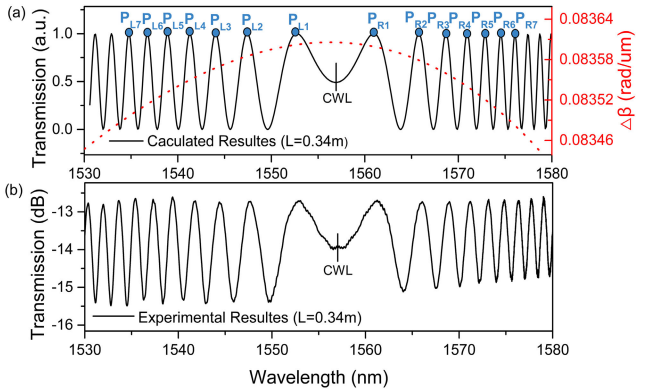

FIGURE 2. Calculated $\Delta\beta$ vs. wavelength, simulated and experimental transmission spectrum of the DMF-MZI structure with straight unstrained 0.34m DMF at a temperature of 25 °C: (a) Calculated results for $\Delta\beta$ and transmission spectrum. (b) Experimental results for the transmission spectrum.

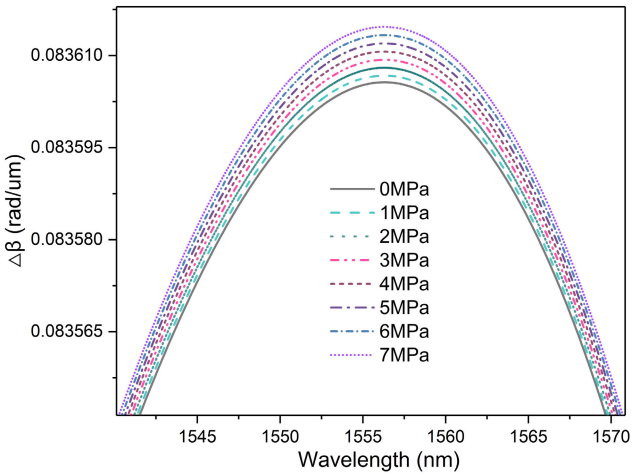

FIGURE 3. Simulated results for $\Delta\beta$, under different pressures, as a function of wavelength.

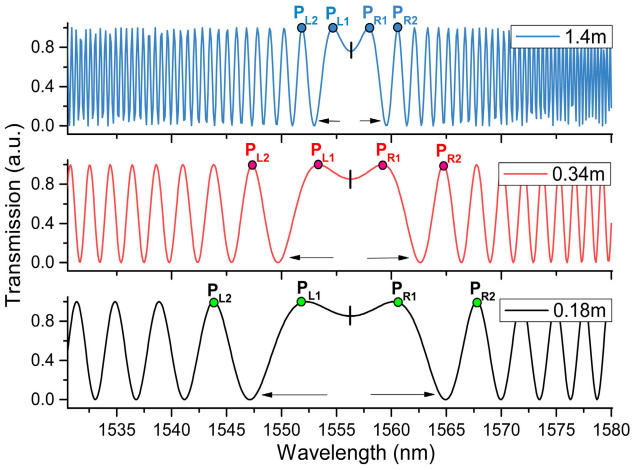

FIGURE 4. Calculated transmission spectra of the DMF-MZI structures employing 0.18m, 0.34m, 1.4m lengths of DMF.

of a Finite Element Method analysis of the optical fiber under the hydrostatic pressure. It should be noted that the values for Young's modulus, $E_{sio_2} = 73.1$GPa and Poisson's ratio, $\upsilon_{sio_2} = 0.17$ are used for the pure silica in these calculations. The axial length elongation, $\Delta L_z = \Delta\varepsilon_z \times L = (\alpha_z/E_{sio_2}) \times L$, where $\Delta\varepsilon_z$ is the strain in the axial direction of the DMF. Assuming that α_z is constant, the pressure-induced elongation in the axial direction, ΔL_z, increases with the increase of the length of the DMF, L, which corresponding contributes to causing a variation in φ (λ).

The results of the simulation of the relationship between $\Delta\beta$ and the wavelength (at a temperature of 25°C) and without axial pressure applied, is depicted as a dashed line in Fig.3. Based on the fact that at the operational wavelength chosen, the dispersion of $\Delta\beta$ exhibits a non-linear behavior and shows a maximum, the periods of the interference fringes closest to the CWL, from both sides, also reach a maximum corresponding to the value of the CWL in the transmission spectrum. Therefore, the high sensitivity obtained is seen when the nearest peak is as close as possible to the CWL. As shown in Fig.4, the periods of the interference fringes closest to the CWL, from both sides, and the maximum wavelength spacing between the Right Peak1 and Left Peak1 decreased with the increase in the DMF physical length. As a result, the position of Right Peak1 and Left Peak1 are closer to the CWL, as the length of the DMF is increasing. Thus, the water pressure sensitivity of DMF-MZI can be further improved by increasing the length of the DMF used.

Assuming the water pressure and temperature sensitivities on the Left Peak1 of the MZI are S_{PL} and S_{TL}, respectively, then with an water pressure variation of ΔP, and a temperature variation of ΔT, the wavelength response of the peak, $\Delta\lambda_{L1}$, to the water pressure and the temperature can be expressed as$\Delta\lambda_{L1} = S_{PL}\Delta P + S_{TL}\Delta T$. For Right Peak1 with pressure and temperature sensitivities of S_{PH} and S_{TR}, respectively, the wavelength response, $\Delta\lambda_{R1}$, to the water pressure and temperature can be expressed as $\Delta\lambda_{R1} = S_{PR}\Delta P + S_{TR}\Delta T$. Thus, the method discussed of simultaneously measuring the water pressure and temperature, using the DMF-MZI structure, can be realized by solving the following sensor matrix equation [37]:

$$\begin{pmatrix} \Delta\lambda_{L1} \\ \Delta\lambda_{R1} \end{pmatrix} = \begin{pmatrix} S_{PL} & S_{TL} \\ S_{PR} & S_{TR} \end{pmatrix} \begin{pmatrix} \Delta P \\ \Delta T \end{pmatrix} \tag{6}$$

The change of water pressure and temperature can be simultaneously determined by use of equations:

$$\begin{pmatrix} \Delta P \\ \Delta T \end{pmatrix} = \frac{1}{D} \begin{pmatrix} S_{TR} & -S_{TL} \\ -S_{PR} & S_{PL} \end{pmatrix} \begin{pmatrix} \Delta\lambda_L \\ \Delta\lambda_R \end{pmatrix} \tag{7}$$

where $D = |S_{PL}S_{TR} - S_{TL}S_{PR}|$ is the absolute value of the determinant of the coefficient matrix. The matrix coefficients can be calculated by making separate measurements of the water pressure and temperature response through the changes in the left/right peak wavelength of the MZI. Therefore, the ambient water pressure and temperature variation can

be determined by the simultaneous measurement of the resonant wavelength changes of the DMF-MZI. According to the error analysis method given by Jin *et al.* [38], if the wavelength measurement resolution of the Optical Spectrum Analyzer (OSA) used is $\delta(\Delta\lambda_{L1})$ and $\delta(\Delta\lambda_{H1})$ at these wavelengths, the theoretical pressure and temperature resolution of the sensor scheme discussed, $\delta(\Delta P)$ and $\delta(\Delta T)$, can be expressed by:

$$\begin{pmatrix}\delta(\Delta P)\\ \delta(\Delta T)\end{pmatrix} = \frac{1}{D}\begin{pmatrix}|S_{TR}| & |S_{TL}|\\ |S_{PR}| & |S_{PL}|\end{pmatrix}\begin{pmatrix}\delta(\Delta\lambda_L)\\ \delta(\Delta\lambda_R)\end{pmatrix} \tag{8}$$

III. EXPERIMENTAL RESULTS AND DISCUSSION

The experimental setup of the hydraulic pressure measurement scheme used is shown in Fig.5. In order to create a practical sensor of this sort, a section of DMF was spliced between two pieces of standard SMF (Coring SMF-28e) to form a MZI structure. The splicing operation was performed by using an automatic fusion splicer (Ruiyan, RYF600P). The DMF-MZI sensor thus created was placed in a commercial hydraulic pressure test chamber (which was provided by the San You Limited Company) and has a measuring range of 0MPa to 7MPa. A supercontinuum laser source (SC-5, YSL Co. Ltd., operating between wavelengths of 480nm-2400nm) was deployed as a broadband light source in this experiment. The transmission spectra obtained were recorded by using an Optical Spectrum Analyzer (OSA, ANDO AQ6317B) with a wavelength resolution of 0.01 nm.

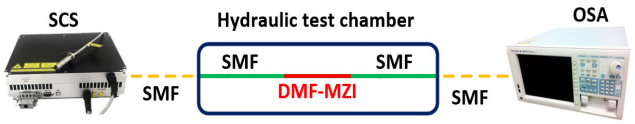

FIGURE 5. Schematic diagram of the experimental setup for water pressure sensing. SCS – supercontinuum laser Source; OSA– Optical Spectrum Analyzer; SMF – single mode fiber; DMF – dual mode fiber; MZI– Mach-Zehnder interferometer.

The sensing responses of the DMF-MZI structure to the water pressure and temperature changes were measured separately for each parameter. The water pressure coefficients were measured while maintaining the room temperature at a value of ∼22°C. The experimental transmission spectra of the DMF-MZI structure (with 0.34m and 1.4m lengths of DMF) monitored when the water pressure increased from 1MPa to 7MPa, are shown in Fig.6 and Fig.8 respectively. It can be clearly observed that the peaks on each side of the CWL shift in opposite directions due to the variation of the water pressure. Moreover, the wavelength shifts, PL1,…, PL7, and PR1,…, PR7, under water pressure changes from 0MPa to 7MPa (with the 0.34m length DMF) are shown in Fig.7. The pressure sensitivity of the DMF-MZI increases dramatically as the peaks approach the CWL, which is experimentally demonstrated in Fig.7 and is consistent with work reported previously by us [26]. The experimental pressure sensitivities monitored as a function of the normalized wavelength of the DMF-MZI sensor, employing different lengths of DMF

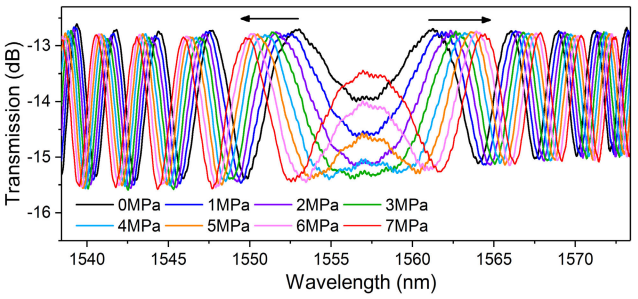

FIGURE 6. Experimental transmission spectra of DMF-MZI structure under water pressures, from 0MPa to 7MPa, with the DMF physical length of 0.34m.

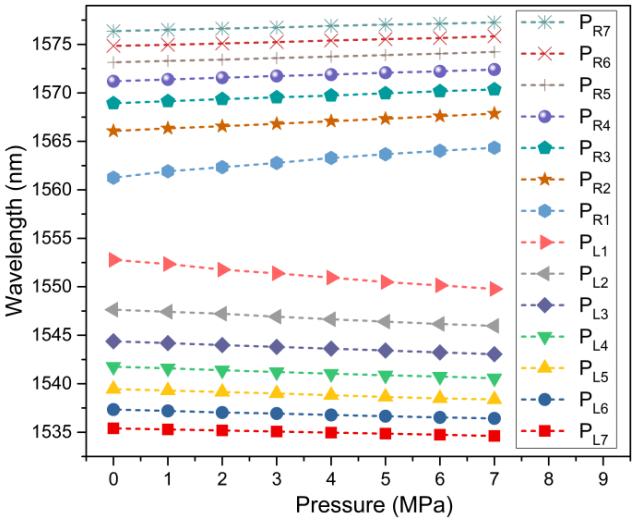

FIGURE 7. Experimental wavelength shifts of peaks in the transmission spectra of the DMF-MZI sensor from the water pressure sensing system with a DMF physical length of 0.34m.

(0.18m, 0.34m, and 1.4m), measured at pressures of 0MPa and 7MPa, were plotted as shown in Fig.9, and these results determined and illustrated here agree well with the simulated results also obtained. In this work, we selected three samples, as exemplars through which to study the transmission spectrum and sensitivity of the DMF-MZI sensor with the different lengths of DMF chosen. Relatively large lengths of TDFs were used in this work, because of the smaller length of DMF corresponding to a larger period of the interference fringes and the space between Left Dip1 and Right Dip1, which are not ideal in the discussion of the characteristics of the critical wavelength interference fringes, in the limited measured spectrum. However, the characteristics of the DMF with lower lengths are also seen to work, in practical applications.

The measurement range demonstrated for the hydrostatic pressure sensor is about 7MPa (this being limited by the test system used) but this upper limit can be further extended for many practical applications. As shown in Fig. 9, the pressure sensitivity of the wavelength peak measured is only relevant to the wavelength spacing of the measured wavelength of the CWL. The physical length of the DMF used in the DMF-MZI sensor and the pressure applied to the DMF

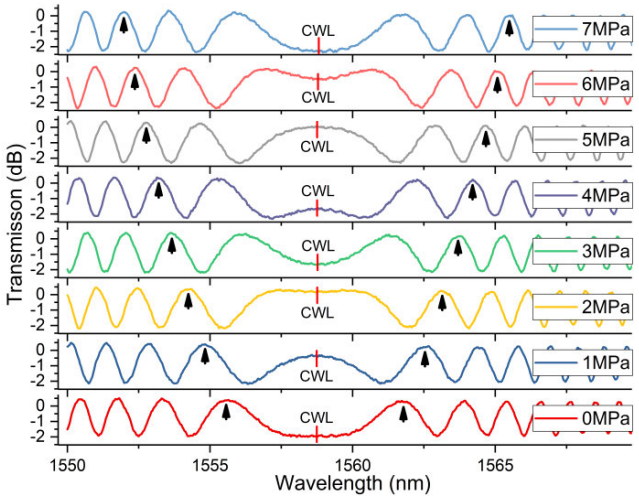

FIGURE 8. Experimental transmission spectra of the DMF-MZI structure under water pressure from 0MPa to 7MPa with the DMF physical length of 1.4m.

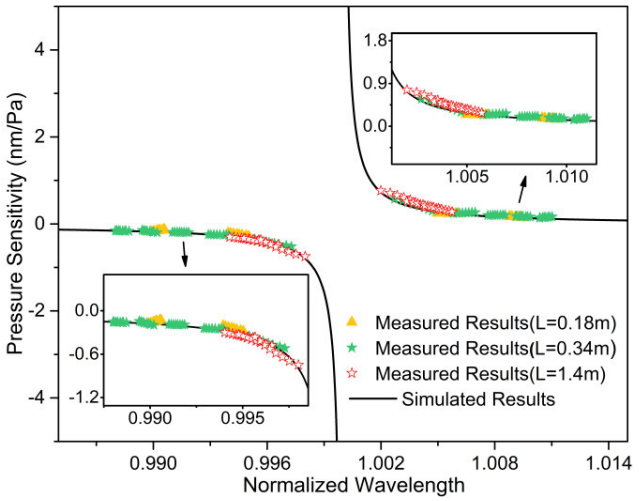

FIGURE 9. The simulated and experimental pressure sensitivities of the DMF-MZI sensor with 0.18m, 0.34m, 1.4m length of DMF vs. the normalized wavelength.

segment may change the wavelength spacing between the peak wavelength and the CWL, thereby affecting the corresponding pressure sensitivity of the peak wavelength measured, as shown in Fig.10. Within the pressure range, 0MPa to 7MPa, the maximum sensitivities of the DMF-MZI sensor (with the 0.18m, 0.34m and 1.4m length of the DMF), measured at Left Peak1 are -0.246nm/MPa, -0.348nm/MPa, and -0.496nm/MPa, respectively. It can be seen that a relatively higher sensitivity is obtained at Right Peak1: 0.251nm/MPa (L=0.18m), 0.437nm/MPa (L=0.34m) and 0.515nm/MPa (L=1.4m), respectively. It is worth noting that the sensitivities of the DMF-MZI structure are effectively improved by increasing the length of the DMF, which are consist with our previous theoretical analysis results.

Moreover, the spacing between Left Peak1 and Left Peak2 measured are 6.945nm (L=0.18m), 5.271nm (L=0.34m)

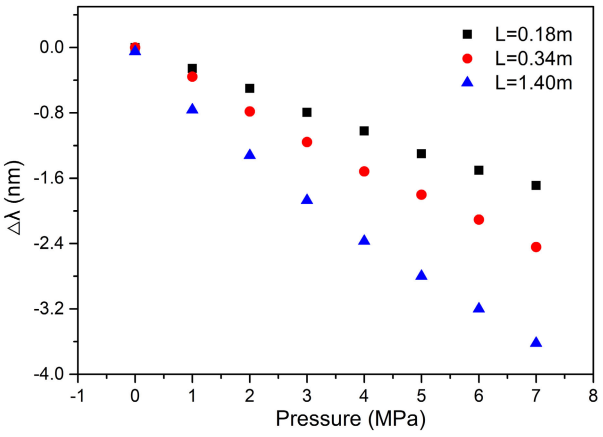

FIGURE 10. Experimental wavelength shifts of Left Peak1 in the transmission spectra of the DMF-MZI with the 0.18m, 0.34m, 1.4m lengths of DMF versus pressure.

and 2.301nm (L=1.4m), respectively, while the spacing between Right Peak1 and Right Peak2 measured are 5.787nm (L=0.18m), 4.775nm (L=0.34m) and 2.174nm (L=1.4m), respectively. It can be noted that the spacing between Left Peak1 and Left Peak2 is slightly larger than that between Right Peak1 and Right Peak2, which corresponds to a relatively larger measuring range of 28.23MPa (water depth=2823.17m), 15.14MPa (water depth=1514.66m) and 4.63MPa (water depth=463.91m), where the lengths of the DMF are 0.18m, 0.34m and 1.4m, respectively. Therefore, in practical applications, the DMF-MZI sensor allows a good compromise between high sensitivity and wide measuring range to be achieved by adjusting the fiber length of the DMF and choosing the measurement peak nearest to a CWL in the transmission spectrum.

The temperature sensitivity measurements of Left Peak 1 and Right Peak 1 were achieved by heating the oven, over the range from 10°C to 30°C. This measurement range covers the temperatures of the composite layer and the thermocline in the tropical and temperate regions of the earth. The lower measuring range (2 – 6°C, with the seawater depth >2000m) could also be further extended in the experiment, with the use of suitable thermostatic equipment. As an example, the DMF-MZI sensor with a DMF length of 0.34m was chosen to illustrate the simultaneous measurement scheme later. The transmission spectrum and the wavelength responses of Left Peak 1 and Right Peak 1 of the DMF-MZI sensor with a DMF length of 0.34m, are shown in Fig.11 and Fig.12, respectively. In a way that is similar to the observed pressure characteristics, over the temperature range from 10°C to 30°C, the Left Peak 1 exhibits a blue shift with a temperature sensitivity of −0.227 nm/°C, while the Right Peak 1 exhibits red shift with a temperature sensitivity of 0.256 nm/°C. A linear regression analysis was used to obtain the correlation coefficients, of >0.992, for all four relationships within a water pressure range of 0–7MPa, over the temperature range studied (from 10 to 30°C).

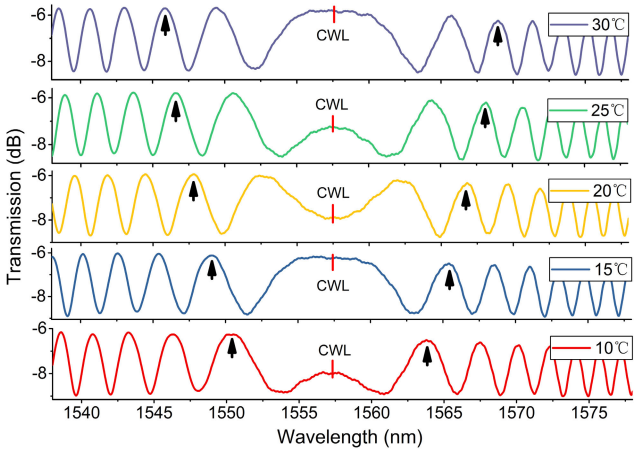

FIGURE 11. Experimental transmission spectra of 0.34m DMF based MZI with the water temperature varying from 10° to 30°.

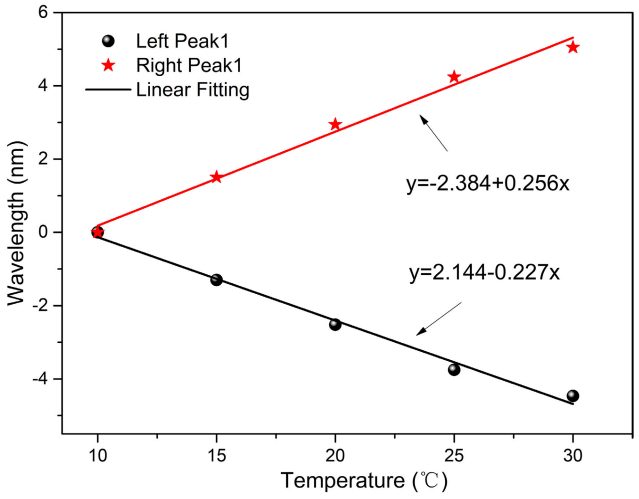

FIGURE 12. Experimentally determined wavelength shifts of Left Peak1 and Right Peak1 in the transmission spectra of the 0.34m DMF-MZI as a function of temperature.

Because the water pressure and temperature coefficients of sensor matrix(7) are $S_{PL} = -0.348$nm/MPa, $S_{PR} = 0.437$nm/MPa, $S_{TL} = -0.227$nm/°C, and $S_{TR} = 0.256$nm/°C, the values of ΔP and ΔT can be calculated by using the following matrix:

$$\begin{pmatrix} \Delta P \\ \Delta T \end{pmatrix} = \frac{1}{0.0101} \begin{pmatrix} 0.256 & 0.227 \\ -0.437 & -0.348 \end{pmatrix} \begin{pmatrix} \Delta\lambda_{L1} \\ \Delta\lambda_{R1} \end{pmatrix} \quad (9)$$

where $\Delta\lambda$ is expressed in nanometers, ΔP in MPa and ΔT in °C. By recording the wavelength response of Left Peak1, $\Delta\lambda_{L1}$ and Right Peak1, $\Delta\lambda_{R1}$, the water pressure and temperature can be measured simultaneously by using the DMF-MZI structure. According to (8), (and using an OSA with a wavelength resolution of 10pm), the theoretical pressure and temperature resolutions of the DMF-MZI sensor obtained, with the DMF length of 0.34m, are 0.047MPa (which are corresponded to water depth of less than 4.7m) and 0.07°C, respectively.

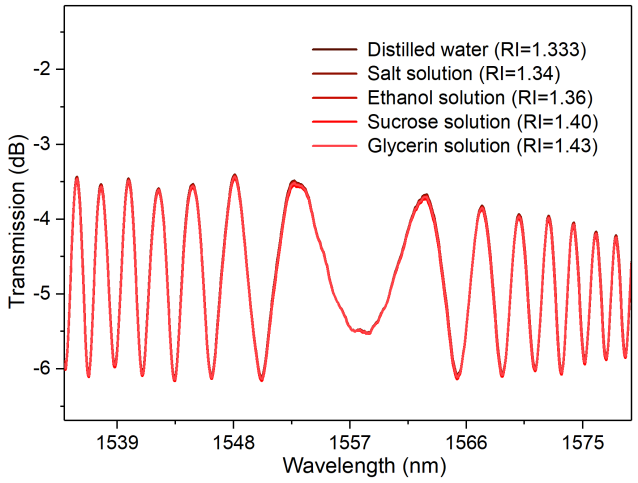

FIGURE 13. Experimental transmission spectra of 0.34m DMF-MZI used with different RI solutions.

Furthermore, the RI response of this DMF-MZI sensor was tested, as shown in Fig.13, with the use of salt/ethanol/sucrose/glycerin solutions and distilled water surrounding on the surface of the fiber. The transmission spectra of the DMF-MZI sensor was hardly changed with the use of those solutions, with different values of RI ranging from 1.333 to 1.43. This arises because the DMF-MZI sensor is based on two core mode interference, of the LP_{01} mode and the LP_{02} mode, which is a very competitive approach when compared to the sensor designs based on the open cavity/bare core/cladding mode/thin clad structure with a large evanescent field spreading on the fiber surface, when applied in the liquid environment. The characteristics of the RI-insensitive nature of the DMF have also been demonstrated when it was to be rolled into a small ring (e.g. the size of a coin), and thus this is an arrangement well suited for both co-located and single point simultaneous multi-parameter measurement.

Further, in practical applications, the edge filter technique could be used to determine the wavelength and thus reduce the cost of it in practical applications, replacing the use of the OSA. The sensing fiber, DMF, supporting only the LP_{01} mode and the LP_{02} mode propagating in the fiber, shows good performance being polarization independent and having an anti-interference characteristic. Thus the DMF-MZI sensor packaged in its free state, is relatively insensitive to water flow changes, variations in the salinity of the seawater or the presence of contaminants in that water.

This innovative MZI sensor structure takes advantage of a simple and co-located sensing structure, the relatively high sensitivities available, and the ease of fabrication and detection discussed. Therefore, it is practicable to use such a DMF-MZI structure-based sensor system to achieve an excellent set of measurements in practice: allowing the simultaneous discrimination of water pressure and temperature, in the sensor device that has been developed and evaluated in this novel work.

IV. CONCLUSION

In conclusion, three DMF-MZI structures with different physical lengths of DMF (0.18m, 0.34m, and 1.4m) were readily formed by splicing a section of DMF-MZI between two segments of SMFs in each case. Those structures, based on two-core mode interference between the LP_{01} and LP_{02} modes, were used for the simultaneous measurement of water pressure and temperature, achieved by monitoring the Left Peak1 and Right Peak1, from both sides of CWL (which shifts in an opposite direction and shows a differential sensibility for both water pressure and temperature variations). The relationship between the pressure sensitivity and the physical length of the DMF has been experimentally and theoretically evaluated in this work. The experimental results obtained show that the DMF-MZI has a linear wavelength shift response to changes in the water pressure and the temperature, and the experimental results obtained are independent of the polarization states of the transmission light, as well as stable with the variation of underwater salinity or impurities seen around the fiber surface. The all-fiber DMF-MZI sensor structure developed in this work also show promising prospects for the simultaneous measurement of pressure (varying due to water depth) and temperature in a wide range of important liquid or gas environmental applications (e.g., natural gas or oil exploitation, etc.), showing the versatility of the sensor approach for various uses by industry.

REFERENCES

[1] N. Bruneau, J. Zika, and R. Toumi, "Can the Ocean's heat engine control horizontal circulation? Insights from the caspian sea," *Geophys. Res. Lett.*, vol. 44, no. 19, pp. 9893–9900, Oct. 2017.

[2] Z. Li, J. Tian, Y. Jiao, Y. Sun, and Y. Yao, "Simultaneous measurement of air pressure and temperature using fiber-optic cascaded Fabry–Perot interferometer," *IEEE Photon. J.*, vol. 11, no. 1, Feb. 2019, Art. no. 7100410.

[3] H. Lin, F. Liu, Y. Dai, and A. Zhou, "Cascaded fiber mach–zehnder interferometers for sensitivity-enhanced gas pressure measurement," *IEEE Sensors J.*, vol. 19, no. 7, pp. 2581–2586, Apr. 2019.

[4] H. Gao, Y. Jiang, Y. Cui, L. Zhang, J. Jia, and J. Hu, "Dual-cavity Fabry–Perot interferometric sensors for the simultaneous measurement of high temperature and high pressure," *IEEE Sensors J.*, vol. 18, no. 24, pp. 10028–10033, Dec. 2018.

[5] L. Zhang, "Simultaneous measurements of temperature and pressure with a dual-cavity Fabry–Perot sensor," *IEEE Photon. Technol. Lett.*, vol. 31, no. 1, pp. 106–109, Jan. 12, 2019.

[6] L. Li, L. Xia, Z. Xie, and D. Liu, "All-fiber mach-zehnder interferometers for sensing applications," *Opt. Express*, vol. 20, no. 10, p. 11109, Apr. 2012.

[7] Q. Wang and G. Farrell, "All-fiber multimode-interference-based refractometer sensor: Proposal and design," *Opt. Lett.*, vol. 31, no. 3, pp. 317–319, 2006.

[8] Q. Wu, Y. Okabe, and J. Wo, "Fiber sensor based on interferometer and Bragg grating for multiparameter detection," *IEEE Photon. Technol. Lett.*, vol. 27, no. 12, pp. 1345–1348, Jun. 15, 2015.

[9] J. N. Dash and R. Jha, "Inline microcavity-based PCF interferometer for refractive index and temperature sensing," *IEEE Photon. Technol. Lett.*, vol. 27, no. 12, pp. 1325–1328, Jun. 15, 2015.

[10] J. Yang, M. Yang, C. Y. Guan, J. H. Shi, Z. Zhu, P. Li, P. F. Wang, J. Yang, and L. B. Yuan, "In-fiber mach-zehnder interferometer with piecewise interference spectrum based on hole-assisted dual-core fiber for refractive index sensing," *Opt. Express*, vol. 26, no. 15, pp. 19091–19099, Jul. 2018.

[11] X. Q. Lei, B. J. Peng, D. R. Chen, Q. G. Shi, and X. W. Ma, "An all-fiber magnetic field sensor based on Dual-S-Shaped optic fiber integrated with magnetic fluid," *IEEE Sensors J.*, vol. 16, no. 4, pp. 958–964, Feb. 2016.

[12] F. Yu, P. Xue, X. Zhao, and J. Zheng, "Simultaneous measurement of refractive index and temperature based on a peanut-shape structure in-line fiber mach-zehnder interferometer," *IEEE Sensors J.*, vol. 19, no. 3, pp. 950–955, Feb. 2019.

[13] H.-K. Kang, H.-J. Bang, C.-S. Hong, and C.-G. Kim, "Simultaneous measurement of strain, temperature and vibration frequency using a fibre optic sensor," *Meas. Sci. Technol.*, vol. 13, no. 8, pp. 1191–1196, Aug. 2002.

[14] W. Wang, X. Zhou, W. Wu, J. Chen, S. He, W. Guo, J. Gao, S. Huang, and X. Chen, "Monolithic structure-optical fiber sensor with temperature compensation for pressure measurement," *Materials*, vol. 12, no. 4, p. 552, Feb. 2019.

[15] N. Dong, S. Wang, L. Jiang, Y. Jiang, P. Wang, and L. Zhang, "Pressure and temperature sensor based on graphene diaphragm and fiber Bragg gratings," *IEEE Photon. Technol. Lett.*, vol. 30, no. 5, pp. 431–434, Mar. 1, 2018.

[16] K. Bremer, T. Reinsch, G. Leen, B. Roth, S. Lochmann, and E. Lewis, "Pressure, temperature and refractive index determination of fluids using a single fibre optic point sensor," *Sens. Actuators A, Phys.*, vol. 256, pp. 84–88, Apr. 2017.

[17] D. Duraibabu, G. Leen, D. Toal, T. Newe, E. Lewis, and G. Dooly, "Underwater depth and temperature sensing based on fiber optic technology for marine and fresh water applications," *Sensors*, vol. 17, no. 6, p. 1228, May 2017.

[18] Y. J. Rao, "Simultaneous strain, temperature and vibration measurement using a multiplexed in-fiber-Bragg-grating/fiber-Fabry–Perot sensor system," *Electron. Lett.*, vol. 33, no. 24, pp. 2063–2064, Jul. 1997.

[19] H. Bae, D. Yun, H. Liu, D. A. Olson, and M. Yu, "Hybrid miniature Fabry–Perot sensor with dual optical cavities for simultaneous pressure and temperature measurements," *J. Lightw. Technol.*, vol. 32, no. 8, pp. 1585–1593, Apr. 2014.

[20] Y.-F. Gu, Y. Zhao, R.-Q. Lv, and Y. Yang, "A practical FBG sensor based on a thin-walled cylinder for hydraulic pressure measurement," *IEEE Photon. Technol. Lett.*, vol. 28, no. 22, pp. 2569–2572, Nov. 15, 2016.

[21] A. G. Leal-Junior, C. A. R. Díaz, A. Frizera, C. Marques, M. R. N. Ribeiro, and M. J. Pontes, "Simultaneous measurement of pressure and temperature with a single FBG embedded in a polymer diaphragm," *Opt. Laser Technol.*, vol. 112, pp. 77–84, Apr. 2019.

[22] M.-F. Liang, X.-Q. Fang, G. Wu, G.-Z. Xue, and H.-W. Li, "A fiber Bragg grating pressure sensor with temperature compensation based on diaphragm-cantilever structure," *Optik*, vol. 145, pp. 503–512, Sep. 2017.

[23] A. M. Vengsarkar and K. L. Walker, "Article comprising a dispersion-compensating optical waveguide," U.S. Patent. 5 448 674, Sep. 5, 1995.

[24] C. Wei, G. Lin, X. Dong, and S. Tao, "A tunable polarization-independent comb filter based on high-order mode fiber," *J. Opt.*, vol. 15, no. 5, Mar. 2013, Art. no. 055403.

[25] C. Lu, J. Su, X. Dong, T. Sun, and K. T. V. Grattan, "Simultaneous measurement of strain and temperature with a few-mode fiber- based sensor," *J. Lightw. Technol.*, vol. 36, no. 13, pp. 2796–2802, Jul. 1, 2018.

[26] C. Lu, J. Su, X. Dong, L. Lu, T. Sun, and K. T. V. Grattan, "Studies on temperature and strain sensitivities of a few-mode critical wavelength fiber optic sensor," *IEEE Sensors J.*, vol. 19, no. 5, pp. 1794–1801, Mar. 2019.

[27] J. Su, X. Dong, and C. Lu, "Property of bent few-mode fiber and its application in displacement sensor," *IEEE Photon. Technol. Lett.*, vol. 28, no. 13, pp. 1387–1390, Jul. 1, 2016.

[28] C. Lu, X. Dong, and J. Su, "Detection of refractive index change from the critical wavelength of an etched few mode fiber," *J. Lightw. Technol.*, vol. 35, no. 13, pp. 2593–2597, Jul. 1, 2017.

[29] X. Lei, X. Dong, and C. Lu, "Sensitive humidity sensor based on a special dual-mode fiber," *IEEE Sensors J.*, vol. 19, no. 7, pp. 2587–2591, Apr. 2019.

[30] S. Rota-Rodrigo, M. Lopez-Amo, J. Kobelke, K. Schuster, J. L. Santos, and O. Frazao, "Multimodal interferometer based on a suspended core fiber for simultaneous measurement of physical parameters," *J. Lightw. Technol.*, vol. 33, no. 12, pp. 2468–2473, Jun. 15, 2015.

[31] T. Liu, J. Wang, Y. Liao, X. Wang, and S. Wang, "All-fiber Mach-Zehnder interferometer for tunable two quasi-continuous points' temperature sensing in seawater," *Opt. Express*, vol. 26, no. 9, pp. 12277–12290, Apr. 2018.

[32] D. Chen, G. Hu, and L. Chen, "Dual-core photonic crystal fiber for hydrostatic pressure sensing," *IEEE Photon. Technol. Lett.*, vol. 23, no. 24, pp. 1851–1853, Dec. 2011.

[33] M. M. Ali, R. Islam, K.-S. Lim, D. S. Gunawardena, H.-Z. Yang, and H. Ahmad, "PCF-cavity FBG Fabry–Perot resonator for simultaneous measurement of pressure and temperature," *IEEE Sensors J.*, vol. 15, no. 12, pp. 6921–6925, Dec. 2015.

[34] P. Lu and Q. Chen, "Asymmetrical fiber Mach–Zehnder interferometer for simultaneous measurement of axial strain and temperature," *IEEE Photon. J.*, vol. 2, no. 6, pp. 942–953, Dec. 2010.
[35] S. M. Tripathi, A. Kumar, R. K. Varshney, Y. B. P. Kumar, E. Marin, and J.-P. Meunier, "Strain and temperature sensing characteristics of single-mode-multimode-single-mode structures," *J. Lightw. Technol.*, vol. 27, no. 13, pp. 2348–2356, Jul. 2009.
[36] C. Wu, B.-O. Guan, Z. Wang, and X. Feng, "Characterization of pressure response of Bragg gratings in grapefruit microstructured fibers," *J. Lightw. Technol.*, vol. 28, no. 9, pp. 1392–1397, May 2010.
[37] M. G. Xu, L. Reekie, J. P. Dakin, and J.-L. Archambault, "Discrimination between strain and temperature effects using dual-wavelength fibre grating sensors," *Electron. Lett.*, vol. 30, no. 13, pp. 1085–1087, Jun. 1994.
[38] W. Jin, W. C. Michie, G. Thursby, M. Konstantaki, and B. Culshaw, "Simultaneous measurement of strain and temperature: Error analysis," *Opt. Eng.*, vol. 36, no. 2, pp. 598–609, Feb. 1997.

XUEQIN LEI was born in Zhejiang, China, in 1990. She received the bachelor's degree in optical information science and technology and the master's degree in optics from Zhejiang Normal University, Zhejiang, China, in 2013 and 2016, respectively. She is currently pursuing the Ph.D. degree in electromagnetic field and microwave technology with Xiamen University, Xiamen, China. Her research interests include optical fiber interferometric sensor designing, fabricating, theoretical studying, and application in marine and industry.

XIAOPENG DONG received the bachelor's degree from Shandong University, in 1983, and the master's degree from the University of Science and Technology of China (USTC), in 1986.

In 1986, he joined the Department of Electronics Engineering and Computer Science, USTC, as a Faculty Member. He visited the Optoelectronics Research Center (ORC), Southampton University, from February 1992 to May 1993, the Department of Electronics Engineering, City University of Hong Kong, from January 1996 to January 1997, and the Department of Engineering Physics, McMaster University, Canada, in 2004. In 1998, he was with the Department of Electronics Engineering, Xiamen University, where he was a Full Professor, in 2000. He has published over 100 journal articles and conference papers. He holds more than ten patents. His research interests include special fibers and optical waveguides, fiber gratings-based components and sensors, interferometric fiber and waveguide devices and sensors, optical fiber current sensor, optical fiber gas sensor, and so on.

CHENXU LU received the bachelor's degree in electronic engineering, the master's degree in electronics and communication engineering, and the Ph.D. degree in electromagnetic field and microwave technology from Xiamen University, Fujian, China, in 2012, 2015, and 2019, respectively.

From 2017 to 2018, she was a Visiting Ph.D. Student with the City, University of London, U.K. She is currently a Postdoctoral Fellow with the City University of Hong Kong. Her work in this article was finished, when she was a Ph.D. Student with Xiamen University. Her research interests include special optical fiber designing, theoretical studying, and application in communication and sensors.

TONG SUN received the B.Eng., M.Eng., and D.Eng. degrees in precision instrumentation from the Harbin Institute of Technology, China, in 1990, 1993, and 1998, respectively, and the Ph.D. degree in applied physics from the City, University of London, in 1999.

She is currently the Director of the Photonics and Instrumentation Research Centre, City, University of London. She also leads research in developing and applying optical fiber sensors and instrumentation to address topical industrial problems. She has authored or coauthored more than 300 scientific and technical articles in journals. She has given many keynote papers with major conferences. She holds over eight patent applications.

Dr. Sun was a recipient of the Callendar Medal and the Oxburgh Medal from the Institute of Measurement and Control, U.K., in 2010 and 2016, respectively, and the Silver Medal from the Royal Academy of Engineering, U.K., in 2016. She received the Officer of the Order of the British Empire from the Queen's 2018 Birthday Honours List for services to engineering, in 2018. She serves as an Associate Editor for *Measurement* (Elsevier). She serves as a Guest Editor for the *Journal of Lightwave Technology*. She also serves on the Editorial Board for the *Journal of Sensor* and the *Journal of Optical and Quantum Electronics*.

KENNETH T. V. GRATTAN received the B.Sc. degree (Hons.) in physics from Queen's University Belfast, Belfast, U.K., in 1974, the D.Sc. degree in sensor systems from the City, University of London, in 1992, and the Ph.D. degree in laser physics in the use of laser-probe techniques for measurements on potential new dye laser systems.

In 1978, he was a Research Fellow with the Imperial College of Science and Technology, to work on advanced photolytic drivers for novel laser systems. In 1983, he joined the City, University of London, as a New Blood Lecturer in physics, where he was a Professor of measurement and instrumentation, in 1991, and the Head of the Department of Electrical, Electronic and Information Engineering. From 2001 to 2008, he was an Associate Dean and the Deputy Dean of the School of Engineering. From 2008 to 2012, he was a First Conjoint Dean with the School of Engineering and Mathematical Sciences and the School of Informatics. In 2013, he was an Inaugural Dean of the City Graduate School. He was a George Daniels Professor of scientific instrumentation, in 2013, and the Royal Academy of Engineering Research Chair, in 2014. He holds several patents for instrumentation systems for monitoring in industry using optical techniques. His work was sponsored by a number of organizations, including EPSRC, the EU, private industry, and charitable sources. He has authored or coauthored over 700 refereed publications in major international journals and conferences. He has co-edited a five volume topical series on *Optical Fiber Sensor Technology*. His work is highly cited by his peers nationally and internationally. His research interests include development and use of fiber optic and optical systems in the measurement of a range of physical and chemical parameters.

Prof. Grattan was the Chairman of the Science, Education and Technology with the Institution of Electrical Engineers (IET) and the Applied Optics Division, Institute of Physics. He is extensively involved with the work of the professional bodies. He was also the President of the Institute of Measurement and Control, in 2000. He has served on the Councils of all three of these professional bodies. He was elected to the Royal Academy of Engineering, U.K. National Academy of Engineering, in 2008, and the President of the International Measurement Confederation, in 2014, and from 2015 to 2018. He received the Callendar Medal from the Institute of Measurement and Control, in 1992, twice the Honeywell Prize for work published from the Institute's journal, the Applied Optics Divisional Prize for his work on optical sensing, in 2010, the Sir Harold Hartley Medal for distinction in instrumentation and control, in 2012, and the Honorary Degree of Doctor of the University from the University of Oradea, in 2014.